

Particle size-dependent fluorescence properties of water-soluble organic compounds (WSOC) and their atmospheric implications on the aging of WSOC

Juanjuan Qin^{1,2}, Jihua Tan^{1*}, Xueming Zhou^{1,3}, Yanrong Yang¹, Yuanyuan Qin¹, Xiaobo Wang¹,
5 Shaoxuan Shi¹, Kang Xiao^{1*}, Xinming Wang²

¹College of Resources and Environment, University of Chinese Academy of Sciences, Beijing, 100049, China

²Guangzhou Institute of Geochemistry, Chinese Academy of Sciences, Guangzhou, 510640, China

³Faculty of Earth Resources, China University of Geosciences, Wuhan, 430074, China

Correspondence to: Jihua Tan (tanjh@ucas.ac.cn); Kang Xiao (kxiao@ucas.ac.cn)

10 **Abstract.** Water-soluble organic compounds (WSOC) ~~are essential~~play important roles in atmospheric particle formation, migration, and transformation processes. Size-segregated atmospheric particles were collected in a rural area of Beijing. Excitation-emission matrix (EEM) fluorescence spectroscopy was used to investigate the sources and optical properties of WSOC. Sophisticated data analysis on EEM data was performed to characteristically estimate the ~~underlying~~ connections among ~~aerosol~~-particles ~~in~~of different sizes. ~~The~~ WSOC concentrations and average fluorescence intensity (AFI) showed
15 monomodal distribution in winter and bimodal distribution in summer, with dominant mode ~~between~~in 0.26 ~~to~~ 0.44 μm ~~for~~size range in both seasons. The EEM spectra of ~~size-segregated~~-WSOC ~~were different among variant~~varied with particle sizes, ~~which could be the results of size, likely due to~~ changing sources and/or chemical transformation of organics. Size distributions of fluorescence regional intensity (region III and V) and humification index (HIX) indicate that humification degree or aromaticity of WSOC was the highest ~~between~~in particle size range of 0.26 ~~to~~ 0.44 μm . The Stokes shift (SS) and the harmonic
20 mean of the excitation and emission wavelengths (WH) reflected that π -conjugated systems were high ~~between 0.26 to 0.44 μm as well in the same particle size range.~~ The parallel factor analysis (PARAFAC) results showed that humic-like substances were abundant in fine particles ($<1 \mu\text{m}$) and peaked at 0.26-0.44 μm . All ~~evidence~~evidences supported that the humification degree of WSOC increased with particle size in submicron mode ($<0.44 \mu\text{m}$) and then decreased gradually. ~~Thus, it was conjectured with particle size, which implied~~ that condensation of organics ~~still goes on~~occurred in submicron ~~mode~~particles,
25 resulting in the highest degree of humification ~~degree exhibit~~ in particle size ~~between~~range of 0.26 ~~to~~ 0.44 μm rather than in $<0.26 \mu\text{m}$. Synthetically analyzing 3-dimensional fluorescence data could efficiently ~~present~~reveal the secondary transformation processes of WSOC.

1 Introduction

The environmental, health, and climate ~~effect~~effects of atmospheric aerosol particles ~~has~~have been reiterated for many years (Pósfai and Buseck 2010; Burnett et al., 2018; Yan et al., 2020), ~~chemical compositions and particle size are crucial for their perniciousness (Johnston and Kerecman 2019; Fan et al., 2020).~~

Water-soluble organic compounds (WSOC is the active fraction of organic particles, comprises) comprise 10% to 80% of organic compounds in atmospheric aerosols (Qin et al., 2018; Almeida et al., ~~2019~~2020; Cai et al., 2020). ~~Previous researchers have proved that~~ WSOC ~~plays a~~play significant ~~role~~roles in cloud formation, solar irradiation, and atmospheric chemistry (Asa-Awuku et al., 2009; Duarte et al., 2019). However, ~~the majority of WSOC remains mysterious, with~~ only 10% to 20% of the organic compounds have been structurally identified, and the majority of WSOC remain uncharacterized. Generally, WSOC mixture contains both aromatic nuclei and aliphatic chains (Decesari et al., 2001; Dasari et al., 2019), ~~incorporating with different highly oxidized~~with functional groups or heteroatoms like hydroxyl, carboxyl, aldehyde, ketone, amino, and other nitrogen-containing groups (Duarte et al., 2007; Cai et al., 2020). Biomass burning and secondary ~~transformation~~transformation of organics ~~were~~are believed to be the main sources of WSOC (ParkSeungShikPark et al., 2017; Xiang et al., 2017).

Many sophisticated analytical techniques have been ~~used~~developed to unveil the chemical ~~structural information~~structure of WSOC (Johnston and Kerecman 2019). Nuclear magnetic resonance (NMR) ~~and mass spectrometry (MS) are two remarkable analytical methods using to structurally unravel the complex WSOC (Duarte et al., 2020). Solution-state and solid-state ^1H NMR, ^{13}C NMR, or two-dimensional NMR are experts~~is a powerful tool in obtaining structures of organics (Stark et al., 2013; Duarte et al., 2015, 2020; Chalbot et al., 2016). ~~Mass spectrometry plays a crucial role in its high sensitivity and molecular specificity (Johnston and Kerecman 2019). Utilization of exquisite mass spectroscopy like Applications of other existing technologies used for identifying organics structure include the~~ electrospray ionization ~~mass spectrometry (ESI-MS), with~~ ultrahigh-resolution Fourier-transform ion cyclotron resonance mass spectrometry (ESI-FT-ICR-MS), ~~and the~~ proton transfer reaction mass spectrometry ~~sees~~(PTR-MS), the Isotopic ratio mass spectroscopy (IRMS), and the accelerator mass spectroscopy (AMS), have been increasing ~~owing to~~because the requirement of further insight into organics in particulate matter (Cai et al., 2020; Mayorga et al., 2021). ~~Isotopic ratio mass spectroscopy (IRMS) and accelerate mass spectroscopy (AMS) are always used to distinguish (2021), and suource distinguishment of organic emissions from fossil combustion sources and/or biogenic sources by carbon isotopic origin~~ (Masalaite et al., 2018; Zhao et al., 2019; Huang et al., 2020). ~~Although having various advantages, the expanding application of formerly~~

~~The above-mentioned instruments is limited by sampling requirements or are generally expensive costs.~~

~~Optical~~to operate. In contrast, optical instruments like ultraviolet and fluorescence spectrophotometers are ~~efficient on~~ examination of organic functional groups in WSOC, some of them are sensitive to quantify the presence of WSOC and its sub-species like brown carbon (BrC) and humic like substances (HULIS)relatively low-cost and efficient. Moreover, data generated by the optical instruments can provide quantitative and qualitative information simultaneously, which warrants their

broad application on organics research, such as investigating WSOC and dissolved organic matter (DOM) in water (Hecobian et al., 2010; Xie et al., 2020). Light absorbing is one of the most important signatures of WSOC (Hecobian et al., 2010). Soleimanian et al., (2020) investigated the chemical properties and spectral properties of aerosol extracts found that the mass absorption efficiency (MAE) was low in the warm season and high in the cold season. The light absorbing method could be used to observe the oxidation dynamics of WSOC for their high efficiency and sensitivity (Zhong and Jang 2014).

Qin et al., 2018; Xiao et al., 2016). 3-Dimensional fluorescence of excitation-emission matrix (EEM) is a sensitive and informative method fluorescence spectroscopy is an optical instrument that has been used in analyzing atmospheric WSOC analysis for several years (Duarte et al., 2004; Fu et al., 2014; Qin et al., 2018; Yue et al., 2019). Fluorescence analysis is a quantitative and semi-qualitative method that mainly investigating can identify chromophoric organics like aromatics, protein, and other organic matters containing π -conjugated systems (Xiao et al., 2018a; Xiao et al., 2018; 2020). EEM is spectrum has been implemented to visualize the fluorescence regions and point out identify possible categories of WSOC by characteristic of fluorescent regions in early years (Duarte et al., 2004; Santos et al., 2009). It could reflect, and to study the aging of WSOC as well, by examining the red or blue shift of fluorescence peaks (Lee et al., 2013; Fu et al., 2015; Vione et al., 2019). 2019). Recent research combined fluorescence spectrophotometry and high resolution structural equipment to verify the chemical information digging from EEM (Chen et al., 2016a). Fluorescence indices are important subsidiary approach approaches to statistically analysis analyze EEM data (Qin et al., 2018; Yue et al., 2019).), which are determined by the chemical structure of pollutants (Andrade-Eiroa et al., 2013a).

Size Earlier studies have investigated size distributions of WSOC are explored for years (Deshmukh et al., 2016; Frka et al., 2018), and more recent studies have interests on the optical properties of size-segregated WSOC (Chen et al., 2019; Yue et al., 2019). Generally, the mass concentrations of WSOC generally show bimodal distributions with the dominant one in the accumulation mode (0.05-2 μ m) (Yu et al., 2004; Yu et al., 2016). Structural investigations on coal burning and biomass burning affected humic-like substances (great parts a significant fraction of WSOC) of in four particle size size ranges found that consistent organic species of specie through all samples were basically the same without size discrepancy, but ranges, however, the absorption bands of aromatic groups were more intense comparing compared to carboxylic groups in sub-3 μ m fractions (Park SeungShik Park et al., 2017; Voliotis et al., 2017). Jang et al., (2019) comprehensively analyzed the structures of size-segregated humic-like substances during extracted from PM_{2.5} in Songdo, South Korea? during periods of pre-, current and post-heating, heating, and after heating periods, and found that CHO, CHON, and CHOS increased in the heating period. The size distribution showed that CHO, CHON, and CHONS species decreased with particle size and the CHOS increased, reversely, indicating the chemical structures of HULIS changed with particle size.

The optical properties of size segregated WSOC arouse increasing investigation recently. Light Liu et al. (2013) examined the light absorption properties of size-resolved brown carbon (BrC in water) and methanol extracts were estimated in urban and rural Georgia, results showed and found that chromophores were predominant in the accumulation mode with an aerodynamic mean diameter of 0.5 μ m (Liu et al., 2013). Fluorescence. More recently, fluorescence properties of size-segregated ambient WSOC and bioaerosols in different particle sizes were estimated in a coal burning city and a mountain site

95 (Chen et al., 2019; Yue et al., 2019). ~~However, enormous information is still hidden in the EEM spectra, not to mention the addition of a size-resolved stratum.~~

~~Among a group~~To date, comprehensive analysis of fluorescence properties of size-resolved aerosols is still very limited, with enormous information being hidden in the EEM spectra. The present study was designed to fill this knowledge gap by investigating the fluorescence properties of WSOC in different particle sizes. Six stage size-segregated particle samples, ~~particles of all formation status~~ were collected in ~~different filters, the neighbor particle sizes might share continuous transformation processes.~~ But the relations of size-segregated WSOC were seldom analyzed before. Taking this in mind, size-segregated particles of winter and summer samples in rural Beijing were collected to investigate the evolution of WSOC. The fast and highly efficient UV-Vis and fluorescence methods were applied in the present research, to obtain the light. Light-absorbing and fluorescent properties of size-segregated WSOC were obtained using the fast and efficient UV-Vis and
100 ~~fluorescence methods.~~ A bunch of fluorescence indices, Stokes shift, and parallel factor analysis (PARAFAC) were performed to quantitatively disclosure the hidden connections and transformations of WSOC. Gary relational degree (GRD) ~~is~~was used to show the relations between particles.
105

2 Method

2.1 Sampling site

110 Size-segregated particle samples were collected by a 6-stage micro-orifice uniform deposit impactor (MOUDI), with aerodynamic cut-point diameters of 0.26, 0.44, 0.77, 1.4, 2.5, and 10 μm , respectively. Sample collection started at 8:00 a.m. till next 7:00 a.m. ~~and was fixed at 23., leaving 1 h to reserve operating time for operation.~~ All samples were collected ~~by on~~ quartz filters (Whatman)), which were prebaked for 5 hours (500°C) ~~and before sample collection, and were~~ wrapped by aluminum foil and stored at -20°C ~~after sampling.~~

115 A total of 20 ~~groups~~sets of 6-stage size-segregated aerosol samples were collected at a rural site in Huairou Distinct, Beijing, from 14 November to 30 December 2016, and ~~from~~ 30 June to 8 September 2017. The sample collection ~~was non-continuous and days were~~ randomly selected ~~and samples were later categorized~~ according to the degree of air pollution. Winter ~~samples sampling days~~ covered ~~6~~six levels of air quality from excellent to severe pollution ~~day, the air quality during, while~~ summer ~~was~~sampling days only covered good and moderate ~~air quality. The air quality index weighted 72h backward trajectories during the sampling period are exhibited in~~ Figure 1.
120

2.2 Chemical analysis

Organic and elemental carbon (OC and EC) were determined by thermal/optical carbon analyzer (DRI), and the thermal evolution protocol IMPROVE (Interagency Monitoring of Protected Visual Environments) was ~~adopted~~adapted. Detailed information ~~could can~~ be found ~~elsewhere in earlier studies~~ (Cheng et al., 2009; Tan et al., 2016). The detection limit of OC and

125 EC was $1.0 \mu\text{g}/\text{m}^3$, as quantified by filter and filter blank. QA and QC were performed by replicate analyses every 10 samples and the repeatability was better than 5%.

A quarter of the filter sample was ultrasonically extracted twice with 5 ml ultrapure water each time and mixed up after extraction. The ~~extract was~~ extracts were then ~~sifted by~~ filtered through a $0.22 \mu\text{m}$ membrane filter to remove impurities: (Xiang et al., 2017). The measurement of WSOC was performed by a TOC analyzer (Analytic Jena AG multi N/C3100, Germany) (Xiang et al., 2017).

The extraction procedures of water-soluble ions (WSIN) were similar to those of WSOC, but using $0.22 \mu\text{m}$ teflon filter to remove impurities. Ion chromatography (IC, Dionex ICS 900 and 1100) was used in the detection, with 8 WSIN species analyzed (Cl^- , NO_3^- , SO_4^{2-} , NH_4^+ , Na^+ , K^+ , Ca^{2+} , and Mg^{2+}). The recovery (90%–110%) and reproducibility (relative standard deviation of each ion lower than 5%) of the ions were implemented as well.

135 2.3 Spectrophotometer Analysis

The extraction procedures of samples subject to fluorescence and ultraviolet-visible (UV-Vis) sampling were the same as for WSOC detection. The excitation-emission spectra were obtained by a fluorescence spectrophotometer (F-7000, Hitachi, Japan), and UV-Vis spectra by an ultraviolet spectrophotometer (UV-2401PC, Shimadzu, Japan). ~~To be brief,~~ Briefly, the wavelength ranges ~~are of EEM were~~ 200–400 nm for excitation and 250–500 nm for emission with 5 nm ~~intervals~~ interval (Qin et al., 2018). UV-Vis was measured with a range of 200–500 nm, with 5 nm ~~intervals~~ interval. All EEM data in the present ~~research study~~ were in Roman Raman unit (R.U., the.). The background signals, interfering signals (first- and second-order Rayleigh and Raman scatterings), and the inner-filter ~~effects~~ effects were removed by subtracting an EEM of blank, ~~replace and replaced~~ with a band of missing values or inserting zeros outside the data area, as detailed ~~procedures could be found~~ in Bahram et al., (2006). Data correction and standardization followed procedures described in Xiao et al., (2016).

145 ~~2.4.1.1~~ As shown in Figure 2, the EEM spectra were partitioned into five regions (Birdwell and Engel 2010), and fluorescence regional integration (FRI) method was applied to examine the fluorescence intensities of the accordant region to the total fluorescence intensity. **Data analysis**

2.4.11.1.1 Fluorescent indices

The EEM data were ~~spectrally corrected by blank sample for instrument bias, inner filter effects, Rayleigh scattering, and most of Raman scatter had been removed.~~ Specific fluorescence intensity (SFI) was the fluorescence intensity divided by WSOC concentrations. ~~Fluorescence is an optical property determined by the chemical structure of pollutants (Andrade-Eiroa et al., 2013a) thus fluorescent indices and partitioning methods were fairish extending to WSOC analysis.~~

2.4 Data analysis

2.4.1 Fluorescent indices

155 Fluorescence indices based on intensity ratios may provide clues about the condensation state of WSOC, ~~such as the humification. Humification~~ index (HIX) ~~was~~ used to reflect the degree of humification (Kalbitz et al., 2000; Coble 2014).

$$\text{HIX} = \frac{\text{EEM}_{\text{Ex}254, \text{Em}435-480}}{\text{EEM}_{\text{Ex}254, \text{Em}300-345}} \quad (1)$$

160 Fluorescence is the light emission of a substance that has absorbed light or other electromagnetic radiation. The energy loss from fluorophore relaxing is expressed as Stokes Shift (SS), ~~the detailed information of SS can be found which was described~~ in Xiao et al., (2019). In brief, ~~the~~ SS is calculated ~~as according to~~ equation (3), ~~2~~ below, where λ_{Ex} is the excitation wavelength and λ_{Em} is the emission wavelength. The harmonic mean of Ex/Em wavelength (WH) in equation (4) could represent the average energy level of excited states. Thus, ~~the~~ SS and WH of each fluorescence intensity could be identified in an EEM spectrum.

$$\text{SS} = \frac{1}{\lambda_{\text{Ex}}} - \frac{1}{\lambda_{\text{Em}}} \quad (2)$$

165 $\text{WH} = 2\left(\frac{1}{\lambda_{\text{Ex}}} + \frac{1}{\lambda_{\text{Em}}}\right)^{-1} \quad (3)$

2.4.2 PARAFAC

~~PARAFAC~~ model can decompose complex EEM spectra into several main components by statistical method. The excitation spectrum, emission spectrum, and scores of each component are as follows:

$$x_{ijk} = \sum_{f=1}^F a_{if} b_{jf} c_{kf} + \varepsilon_{ijk}, \quad i=1, \dots, I; \quad j=1, \dots, J; \quad k=1, \dots, K \quad (4)$$

170 ~~Where~~ x represents the fluorescence intensity, f is the number of components resolved by PARAFAC, a is proportional to the concentration of the f -th component, ~~and~~ b and c are the scaled estimating of the emission and excitation spectra. ~~Footnote of The subscript~~ i is the sample number, ~~footnotes and~~ j and k represent emission and excitation ~~wavelengths wavelength~~, respectively. Before performing PARAFAC, all EEM data were normalized to unit norm to ~~reducing reduce~~ concentration-related collinearity and avoid extremely different leverages (Wang et al., 2020). ~~Tucker congruence coefficient (TCC) was determined for each excitation spectrum and emission spectrum, and a threshold of 0.95 was applied to confirm the spectral congruence. The model was determined by half-split validation.~~

175

2.4.3 Grey relational analysis (GRA)

~~Grey relational analysis (GRA) is a part of the grey system theory proposed by Deng (1982), that which can be used to describe the relative changes among factors in a system development process. To perform GRA analysis, references and comparison sequences should be selected and converted to the dimensionless format. The grey relational coefficients~~ ~~The detailed calculation of the series and grey relational degree are calculated as follows.~~

180

$$\xi_i(k) = \frac{\min_k \min_k |y(k) - x_i(k)| + \rho \max_k \max_k |y(k) - x_i(k)|}{|y(k) - x_i(k)| + \rho \max_k \max_k |y(k) - x_i(k)|} \quad (5)$$

$$GRD_i = \frac{1}{n} \sum_{k=1}^n \xi_i(k), \quad k = 1, 2, \dots, n \quad (6)$$

In which y is the (GRD) was explained in the supplementary information. Generally, in GRA, a reference sequence and x_i ($i=1,2,3,\dots$) is the line and one or a series of comparison sequences were selected, and GRD between the reference line and comparison sequences, ρ is the distinguishing coefficient always set as 0.5, ξ_i the grey relational coefficients of individual sample of the series, and GRD_i is the grey relational line indicated the compactness degree calculated by the average of ξ_i (Qiu et al. 2012). The fluorescence intensity is highly affected by WSOC concentration and many other factors, but their exact relations are not clear, thus it could be properties of WSOC were considered as a grey system and. Two sets of GRA were performed for the WSOC of each season. Firstly, considering the evolution of particle size as a changing system, larger particles might come from accumulation and transformation of smaller particles, especially for ultrafine particles. By setting data of particles smaller than 0.26 μm (WSOC concentrations, AFI or UV) as references and particles larger than 0.26 μm as comparisons, their affinities were analyzed by GRA method. Secondly, the fluorescence spectra were generated by part of WSOC, setting the WSOC concentration as a reference and AFI (or UV) as a comparison. The relations between WSOC and AFI for six stage particles were analyzed.

3 Results

3.1 Chemical compounds of size-segregated particles

3.2.3.1 Table 1

Table 1 showed shows the size-segregated mass concentrations of WSIN, WSOC, and OC, and their ratios generated from the data collected at a rural site in Beijing for during winter and summer. WSOC showed a feature of monomodal in winter and bimodal features in summer, respectively, with a dominant mode between 0.26 to 0.44 μm , or having in both seasons and a small secondary mode in particles larger than 1 μm in summer, indicating that carbonaceous species were mainly rich in fine particles (Huang et al., 2020). Contemporary reports by other researchers observed bimodal distribution of organic matter WSOC with two peaks located at 0.8 μm and 7 μm , respectively, in Shenzhen, China, and 0.4-0.5 μm and 2-3 μm in Gwangju, Korea (Yu et al., 2016; Huang et al., 2020).

The WSOC/OC ratios were 0.24 to 0.56 in winter and 0.16 to 0.31 in summer, which was lower than the previous records of the. These values were smaller than those previously reported for a polluted period in Beijing, and they were also lower than those of in the other cities in China (Tian et al., 2014; Wu et al., 2020). Earlier studies suggested higher WSOC/OC ratios

in summer than winter (Xiang et al., 2017; Qin et al., 2018), which is in contrast to the results of the present study. Contrasting seasonal patterns in WSOC/OC ratios were also reported between urban and rural sites in Georgia, US (Zhang et al., 2012), which seemed to support our results presented above. The WSOC/OC ratios were ~~high~~higher in ~~fine~~ particles with an aerodynamic ~~diameters lower~~diameter smaller than 1.4 μm ~~and were low~~than in coarse mode ($\text{PM}_{2.5-10}$), which was accordant with ~~former research on findings previously reported for~~ clear days in Beijing (~~characteristic of organic pollution in the size-segregated aerosol~~ Tian et al., ~~2016~~)'s results).

3.3.2 Excitation-emission spectra of size-segregated WSOC

The size-segregated EEM spectra of winter and summer WSOC ~~were~~are depicted in ~~Figure 2~~Figure 2 (a) and (b), ~~respectively, and~~ their fluorescence intensities ~~of~~-per unit WSOC (SFI) ~~were plotted~~are in (c) and (d), respectively. ~~The bulk fluorescence features of WSOC showed evident distinctions among fine particles and coarse mode particles on EEM spectra. They differed from the spectra of TSP samples in Japan and $\text{PM}_{2.5}$ samples in an industrial city of China, as well (Chen et al., 2016a; Qin et al., 2018), indicating that sources affected the fluorescence properties of WSOC. The fluorescence intensities were highest in particle sizes between 0.26 to 0.44 μm during winter and summer.~~

Interesting characteristics were found in SFI spectra and they could reflect the fluorescence density of WSOC (Xiao et al., 2016). ~~SFI spectra of coarse mode WSOC (which were accordant with natural sources of our unpublished research) didn't show much seasonal difference, but the SFI spectra of fine particles (matched with anthropogenic sources and secondary sources of our study) showed distinctiveness both with altering particle sizes and seasons. Especially, in winter, the SFI spectra showed a clear blue shift within region I to III when particle size increasing, while they showed humble variations in summer.~~

Figure 3 was the size distributions of WSOC and average fluorescence intensity (AFI) in winter and summer, respectively. ~~AFI showed monomodal distribution with peaks between 0.26 to 0.44 μm in winter, and bimodal distribution in summer, which was accordant with WSOC. AFI/WSOC ratios could represent the overall average fluorescence density of WSOC (Xiao et al., 2016). The AFI/WSOC ratios ranged from 0.22 to 0.57 in winter and 0.18 to 0.34 in summer, respectively. And they were higher than that in the industrial city of Lanzhou (Qin et al., 2018). Our unpublished research found that the AFI/WSOC ratios were lower than 0.2 for anthropogenic source samples, indicating that this ratio might be higher in oxidized fluorescent WSOC.~~

The overall fluorescence peaks of EEM were mainly produced among regions II-V and the peaks were peak A, peak T, and peak M, which could be categorized as humic-like, tyrosine-like, and oxygenated organic substances, respectively (Qin et al., 2018). ~~The fluorophores first increased with increasing particle size and reached the highest intensities at particle sizes of 0.26-0.44 μm , and then decreased with increasing particle size in both seasons. Although the fluorescence peaks of WSOC were mainly produced at similar regions between the two seasons, the relative abundance was different (more quantitative analysis below). The aggregated fluorescence spectra of all size-segregated samples resembled the spectra of TSP and $\text{PM}_{2.5}$ shown in Figure S1 with some subtle nuance in border shape (Chen et al., 2016a; Qin et al., 2018).~~

The detailed characteristics of EEM intensity could be found in SFI spectra. The SFI showed evident differences between fine and coarse mode particles in both seasons. The spectra of coarse mode WSOC covered a wide range of natural sources (according to our unpublished research), while the spectra of fine particles widely overlapped with that of PM_{2.5} in Figure S2 (matched with anthropogenic sources and secondary sources of our study), indicating that sources of WSOC affected its fluorescence properties. Besides, the SFI spectra showed a clear blue shift within regions I to III with increasing particle size in winter, and showed humble variations in summer.

Figure 3 shows the size distribution of WSOC and its average fluorescence intensity (AFI) in the two seasons. AFI showed monomodal distribution with peaks in particle sizes of 0.26-0.44 μm in winter, and bimodal distribution in summer, which was accordant with the size distribution of WSOC. AFI/WSOC ratios could represent the overall average fluorescence density of WSOC (Xiao et al., 2016). The AFI/WSOC ratios ranged from 0.22 to 0.57 in winter and from 0.18 to 0.34 in summer. These values were higher than that in the industrial city of Lanzhou (Qin et al., 2018). Our unpublished research found that the AFI/WSOC ratios were lower than 0.2 for anthropogenic source samples.

Fluorescence regional integration (FRI) was calculated to quantify the relative strength of fluorescence intensity on regions I-V, represented by FRI1-FRI5. ~~The FRI of each region was depicted in~~ (Figure 4. ~~To be brief,~~). FRI I and FRI II (protein-like) ~~increase species~~ increased with increasing particle size and peaked at coarse mode in winter. FRI III and FRI V (HULIS) were ~~the most mainly~~ abundant ~~two fluorophores rich~~ in fine particles. FRI IV (microbial related species) ~~peaked between 1.4 to 2.5 μm and~~ showed little variations in particle size range of 0.26-2.5 μm , but decreased with particle size increase. ~~Almost the same size distributions from 2.5 to 10 μm . In summer, the sum of protein-like (FRI I to FRI III increase with particle size increasing, peaked at 1.4 μm and decreased with particle sizes from 1.4 to 10 μm . FRI IV showed reversely tendencies and microbial species) decreased with particle size in the range of 0.26 to 1.4 μm , and HULIS fluorophores were also obtained by the isotopic method (Huang et al., 2020), increase in particle size range of 1.4 - 10 μm . FRI V didn't have a clear tendency but they showed high portions among 0.26 to 0.44 μm and 0.77 to 1.4 μm .~~

3.4.3.3 Fluorescent indices and ~~deep~~ properties associated with fluorescence mechanisms

Inclusive information was stored in EEM spectra, with some regularities ~~were being~~ extracted by performing division of fluorescence intensities between wavelengths. Humification index (HIX) represents the humification degree or aromaticity of fluorescent organics. Peak T/Peak C ~~was~~, the ratio between tryptophan and humics, ~~suggesting can reflect~~ the biodegradability of organics. ~~Some other fluorescence indices are listed in Table S1. Figure 5 showed shows~~ the size distribution of HIX and Peak T/Peak C ratio ~~in this research.~~ HIX showed monomodal distribution ~~and peaked~~ ~~peaking~~ between 0.26 to 0.44 μm in summer and 0.44 to 0.77 μm in winter, indicating the aromaticity of size-segregated WSOC increased ~~firstly first~~ and ~~then~~ decreased afterwards ~~with increasing particle size~~. Peak T/Peak C ~~ratios of different particles ratio~~ increased gradually with increasing particle size in winter, while in summer, ~~they it~~ decreased ~~firstly first~~ in fine particles and then increased ~~with particle size~~. Peak T/Peak C peaked at coarse mode in both seasons, indicating that fluorescent ~~biogenic organics were~~ ~~microbial~~

275 ~~related species~~ likely ~~to exist~~ existed in ~~larger~~ large atmospheric particles. ~~Former researchers also found~~ It was reported that biogenic oxygenated organics are more inclined to ~~sink in~~ adhere to coarse mode ~~particles~~ (Huang et al., 2020).

Stokes shift (SS) is the energy loss of fluorophore relaxation, which might ~~associate~~ be associated with the ~~conjugated~~ π -conjugated system and electron cloud density (Lakowicz, 2006). ~~Xiao et al., (2019) found that Stokes shift of 1.2 μm^{-1} is an important border of hydrophobic and hydrophilic components.~~ High SS ~~indicates~~ values indicate greater energy loss due to relaxation in the excited states, ~~organic~~. Organic compounds having larger π -conjugation scales are possibly exhibit high fluorescence intensity in the high SS region (Xiao et al., 2020). ~~The Xiao et al., (2019) found that SS near 1.2 μm^{-1} is an important border of hydrophobic and hydrophilic components. Hydrophobic fractions tend to have higher intensity in SS > 1.2, possibly as a result of the large scale of the π conjugated system. In contrast, hydrophilic fractions usually have ionogenic groups bond with fluorescent aromatics reduced π -conjugated systems, hence, leading to high fluorescence intensities existing on both sides of SS of 1.2. Note that the same research also reported earlier that hydrophobic fractions tended to present fluorescence peaks at SS > 1 (Xiao et al., 2016). Thus, the~~ ratios of fluorescence intensity in high SS ($\text{SS} > 1.1$) are calculated as ~~the followed equation follows:~~

$$\eta_{\text{SS} > 1.1} = \frac{\sum_{\text{Ex}} \sum_{\text{Em}} I |_{\text{SS} > 1.1}}{\sum_{\text{Ex}} \sum_{\text{Em}} I} \quad (7)$$

The harmonic mean of the excitation and emission wavelengths (WH) reflects the average energy level of the excited states. On a large ~~scale of a~~ π -conjugated system, the electron in the ground state needs ~~lower~~ relatively low excitation energy jumping to the excited state (~~Valeur and~~ Berberan-Santos and Valeur, 2012). The ratios of fluorescence intensity in low energy state ($\text{WH} > 320$) are calculated as ~~the followed equation follows:~~

$$\eta_{\text{WH} > 320} = \frac{\sum_{\text{Ex}} \sum_{\text{Em}} I |_{\text{WH} > 320}}{\sum_{\text{Ex}} \sum_{\text{Em}} I} \quad (8)$$

Size-segregated SS, average SS, ~~and~~ $\eta_{\text{SS} > 1.1}$, ~~and~~ $\eta_{\text{WH} > 320}$ ~~were plotted are shown~~ in Supporting information Figure 3, S4 and Figure 5(c). ~~SS of all particle sizes showed similar distributions, in terms of the consistency of fluorescence energy for WSOC. The intensities for SS < 1.1 were of the same level as those for SS > 1.1, indicating the predominance of hydrophilic fluorescent contents in WSOC. The average SS showed unobtrusive variations with increasing particle size increase in both seasons, and $\eta_{\text{SS} > 1.1}$ was slightly higher in particle sizes < 1.4 μm than other particle size, in winter. $\eta_{\text{WH} > 320}$ tended to increase between from particle size size 0.26 to 0.44 μm and then decrease afterwards in both in winter and summer, (Figure 5c), indicating existence of a larger large scale of the π conjugated system or higher high π -electron density in submicron particles around 0.44 μm , and decreased with particle increasing size in 0.44 to 10 μm .~~

3.5.3.4 EEM fluorophore revealed by classification of PARAFAC results

Parallel Factor Analysis (PARAFAC) is a mathematical method ~~that~~ capable of ~~separates~~ separating chemically independent but spectrally overlapping fluorescence components, ~~based~~ on the ~~basic~~ assumption that EEM spectra are independent, liner related, and additive (Murphy et al., 2011). Several prior studies have been carried out using the PARAFAC method ~~investigating to investigate~~ fluorescent WSOC in ~~aerosol atmospheric aerosols~~ (Pohlker et al., 2012; Chen et al., 2019; Yue et

al., 2019). Results showed that bioaerosols exhibited high bimodal signals at excitation wavelength 275nm, and emission wavelength 320nm, which is sorted as protein-like organic matter. While in a typical coal burning city of China, fluorophores emerging at excitation wavelength 230-250nm and emission wavelength 380-410nm were associated with humic-like substances with larger molecular weight.

The present study produced PARAFAC analysis separately for winter and summer samples, for the separately to reveal seasonal diversities of dependent EEM spectra. Three components were extracted from winter EEM spectra, including C1 was defined as HULIS-1, C2 was representing a protein-like component, and C3 was defined as HULIS-2 (Chen et al., 2016b). However, there were just only two recognizable components C1 and C2 were identified in summer which were, with C1 characterized as HULIS-1 and C2 as protein-like components, respectively. Component C3 in summer EEM spectra was of no physical significance (multiple emission peak points at one single excitation wavelength) and characterized as a noise signal.

The portions of the extracted components were plotted below are also shown in Figure 6 together with PARAFAC results in Figure 6. Protein-like compounds were more abundant in particles larger than 2.5 μm on both seasons (37%-40% in winter and 20%-21% in summer, respectively), and HULIS showed higher fractions in fine mode and was low in than coarse mode particles on two in both seasons, which quantitatively demonstrated that biogenic microbial related WSOC were more likely to exist existed in large particles and HULIS was rich in fine mode particles. The ratios of HULIS-1 and HULIS-2 were defined in winter, their ratios HULIS-1 / HULIS-2 were low in ultrafine particles ($<0.26\mu\text{m}$) and coarse mode, and high were higher in fine particles with an aerodynamic diameter ranging between of 0.44 to $2.5\mu\text{m}$, than in ultrafine particles ($<0.26\mu\text{m}$) or coarse mode particles. HULIS-2 was likely to be freshly emitted fluorescent WSOC and HULIS-1 exhibited fluorescent characteristics of oxidized HULIS (Vione et al., 2019). The low HULIS-1 / HULIS-2 ratios in ultrafine and coarse mode particles might be due to abundant sources of freshly emitted WSOC.

3.6.3.5 Specific relations among size-segregated WSOC and fluorescence properties weighted by Grey Relational Degree (GRD)

Grey relational analysis (GRA) GRA method is suitable for solving problems with complicated interrelationships between multiple factors and variables (Morán et al., 2006). The principle of GRA is to estimate the similarity and degree of the compactness among factors based on the geometric shape of the different sequences (Deng 1989). It has been used on multiple attribute decision-making problems for solving environmental issues (Kuo et al., 2008), evaluation of air quality control policy (Xu et al., 2011; You et al., 2017), and influencing factor determination of microbial product formation processes (Xu et al., 2011). GRA method). GRA was performed in the present research because study considering that atmospheric particles can be considered treated as a grey system for their high complexity and indeterminacy.

The GRD of size-segregated WSOC, AFI, and average UV were shown in Figure 7 (a) and (b). High GRD always refers to represents high connections connection between referencing and comparing factors. By setting WSOC (or AFI and UV) of particles $<0.26\mu\text{m}$ as references, (a) and (b) in Figure 7 depicted the and those of larger particles as comparisons, relations

340 among particle sizes ~~in winter and summer, respectively. They can be depicted by~~ GRD of ~~size-segregated~~ WSOC, ~~(or AFI, and~~
~~UV-between particle sizes were basically well among both seasons),~~ as shown in Figure 7(a) for winter samples and Figure
7(b) for summer samples. In winter, GRD_{0.44} to GRD_{2.5} showed a downward tendency varying from 0.88 to 0.76 for WSOC
and 0.88 to 0.78 for AFI, indicating that WSOC concentration and AFI gradually ~~“dislike”~~ deviating from their original
situation with increasing particle size ~~increasing~~. In summer, GRD_{0.44} to GRD_{2.5} showed little variations with average values
345 at 0.64 for WSOC and 0.73 for AFI, but decreased in GRD₁₀, indicating that WSOC in ~~coarse mode was different~~ particles
larger than 0.26 μm had little inheritance from ~~that in the primal~~ fine particles.

The relations between WSOC and ~~its optical properties were showed~~ AFI and average UV (referred to as UV below) of
different particles are shown in Figure 7 (c) and (d) ~~for winter and summer, respectively~~. AFI and ~~average~~ UV showed high
GRD ~~among in~~ both seasons for all particle sizes (with average GRD>0.9), indicating that fluorescence intensity and light
350 ~~absorptions~~ absorption were closely connected with WSOC ~~concentrations~~ concentration. However, clear variations of GRD
were observed with increasing particle size ~~increasing~~. ~~It was with contrasting patterns to those of fluorescence indices. Thus,~~
~~it was~~ speculated that these variations were ~~resulting~~ resulted from secondary ~~transformation~~ transformation of WSOC ~~because~~
~~GRD were, as indicated by fluorescence indices. Besides, GRD~~ strongly negatively correlated with estimated secondary
organic carbon (SOC) ~~concentrations~~ concentration with a correlation efficient r ~~at of~~ -0.64 ($p<0.000$) in winter and -0.63 in
355 summer. The lowest GRD was found for particle sizes ~~between of~~ 0.26 to 0.44 μm , ~~combining with former results of. The~~
high AFI, large π -conjugation ~~scales, and more~~ scale, rich HULIS ~~also observed, and low GRD~~ in this particle size range, ~~it~~
~~was concluded~~ indicated that fluorescent WSOC ~~in particle sizes between 0.26 to 0.44 μm of these particles~~ was highly affected
by secondary processes ~~and. Thus,~~ GRD between WSOC and AFI could serve as an ~~indicator~~ indicator of secondary formation.

4 Discussion

360 By characteristically analyzing the fluorescent properties of size-segregated WSOC, we have gained a better understanding
of the ~~hiding~~ hidden relations between fluorescence and WSOC ~~concentrations~~ concentration, the possible evolution of
fluorescence properties during particle size increase ~~growth~~, and the source distinction of fluorescent WSOC ~~in~~ between fine
and coarse particles ~~were getting clear~~.

Accordant with ~~former research~~ earlier reports, the fluorescence intensities ~~were~~ positively ~~related to~~ correlated with WSOC
365 concentrations in both ~~in~~ winter and summer (Spearman's $r>0.8$, $p<0.001$) (Qin et al., 2018; Chen et al., 2019). The size
distributions of AFI kept in step with those of WSOC concentrations and showed monomodal ~~distribution~~ distributions in
winter and bimodal ~~distribution~~ distributions in summer ~~peaked, peaking~~ in particle sizes between 0.26 to 0.44 μm (Figure 2
(a) and (b)). The EEM spectra of size-segregated WSOC mainly ~~exhibit~~ exhibited among regions 2-5 ~~II-V~~ and ~~they~~ blue-shifted
with increasing particle size ~~increase~~ (0.44 to 10 μm), ~~which could be obviously observed from the EEM spectra and the~~
370 ~~increase of FRI1 and FRI2 and decrease of FRI3 and FRI5. These phenomena are explained below.~~

The SFI spectra (fluorescence intensity per unit WSOC) showed different properties ~~amongin different~~ seasons ~~andor~~ particle sizes. The size-segregated AFI/WSOC ratios were relatively high in fine particles with sizes between 0.26 to 1.4 μm (mainly affected by anthropogenic sources and secondary process) and low in large particles ($\text{PM}_{2.5}$), but ~~theyall~~ were ~~both~~ higher than ~~that inthose of~~ source samples. Freshly emitted WSOC from the source sample ~~containscontain~~ more unsaturated groups like aromatics and ~~hashave~~ lower O/C than the ~~long-transported-sampleaged ones~~ (Zhang et al., 2018, Cai et al., 2020). Substitution and oxidation reactions of ambient organics might widen the delocalization of π electronics and reduce the excitation energy, thereby resulting in a redshift of EEM spectra (Kalberer et al., 2004). The specific fluorescence area was widened in ~~the~~-ambient sample and thus ~~havinghad~~ a higher AFI/WSOC ratio when WSOC concentrations ~~were~~ at a comparable level. ~~ContinuouslyContinuous~~ oxidation of organics may break up the π system of organics and extinct fluorescence (Zanca et al., 2017). It could be inferred that ambient WSOC ~~tendingtended~~ to exhibit higher AFI/WSOC ratios, while both freshly emitted WSOC and completely ~~oxidization-ofoxidized~~ WSOC could lead to ~~a~~-lower AFI/WSOC ~~valuevalues~~.

The fluorescence indices showed ~~clear particle size-dependent changes and~~ vague seasonal variations. ~~SameThe same~~ tendencies, ~~i.e.,~~ increased first~~and decreased afterwards~~ (~~peaked in particle size between 0.22 to 0.44 μm , and then decreased with particle size~~), were observed in fluorescence indices of HIX and $\eta_{\text{WH} > 320}$, indicating that the π -conjugated system of WSOC increased ~~first~~ and ~~then~~ decreased ~~thenwith particle size~~. Besides, in the EEM spectra, peak M was strong in particle sizes lower than 0.77 μm and bleached in larger particles, ~~and~~ peak A blue-shifted with ~~increasing~~ particle size~~-increase~~. Contemporary research also found that aromatic secondary organic aerosol increased during the haze period (Yu et al., 2019). ~~Besides, it was noticed that HIX and WSOC/OC showed similar size distributions except for larger peaking particle size of WSOC/OC values comparing to HIX. Because the fine particles with relatively large sizes could long exist in atmospheric environment, the WSOC/OC ratios increase gradually, however, the oxidation process could also cause fluorescence quenching and lead to the decrease of HIX (Vione et al., 2019). Thus, HIX peaked in smaller particle size comparing to WSOC/OC.~~

All evidence on EEM ~~propertiespectra~~ and fluorescence indices ~~discussed~~ above suggested that the aging of WSOC might have experienced ~~two~~-evolution processes of ~~increase and decrease with~~-particle size ~~increasingchanges~~. In the ~~first~~-process ~~of~~ ~~particle size increase~~, fluorescence and π -conjugated system increased and peaked between 0.22 to 0.44 μm , and peak M sparkled. Two possible ~~pathwaysmechanisms~~ were proposed to explain this phenomenon. The first ~~conjectureone~~ was ~~that~~ heterogeneous polymerization of gas and liquid phase organics enlarged the delocalization of π electrons and ~~leadingled~~ to the increase of fluorescence (Kalberer et al., 2004). De Laurentiis et al. (2013) found that the triplet state of 1-nitronaphthalene directly ~~reactsreacted~~ with phenol and ~~formingformed~~ biopolymer transformation intermediates in the liquid phase, ~~and~~ the fluorescence spectra shifted to peak “M” during irradiation. The second ~~conjectureone~~ was that during oxidation processes of organics in small particles, oxygen heteroatomic rings formed or chromophoric groups like $-\text{NO}_2$ and $-\text{OH}$ added to the fluorescent organics~~-increased~~, ~~which both could increase~~ the π -conjugated system. Lee et al., (2014) observed that fluorescence ~~increased in solar irradiation experimentsintensity~~ of secondary organic aerosol ~~preparedproduced~~ by high- NO_x photooxidation of naphthalene (NAP SOA)~~-increased when they were solar irradiated~~. In the ~~second~~-process ~~of~~ ~~particle size~~

405 ~~decrease~~, fluorescence decreased with ~~partiele-size~~-increasing particle size and peak M dribbled away. This might be because ~~the~~ further oxidation process gradually broke up the aromatic rings or unsaturated bonds in organic matters and ~~not fluorescent~~. fluorescence quenched. Laboratory results also confirmed that after a long period of irradiation the fluorescence intensity of fluorescent organic decreased eventually (De Laurentiis et al., 2013, Lee et al., 2014).

PARAFAC results showed that HULIS was rich in fine particles and protein-like compounds were rich in coarse particles amongin both seasons, which were accordant with ~~former research~~earlier reports (Chen et al., 2019; Huang et al., 2020). In winter, the wavelength of HULIS-1 was slightly higher than ~~that of HULIS-2 and their~~. The EEM spectra of HULIS-1 observed in the present study were similar to the PARAFAC results of highly oxygenated species ~~and~~, while those of HULIS-2 to less oxygenated species reported in Chen et al (2016b)'s study on the chromophoric WSOC. Only HULIS-1 was distinguished in summer ~~and it in the present study, which~~ could be allocated to highly oxygenated species. ~~The sources of HULIS and protein-like compounds might be fossil fuel oxygenated organic carbon (OOC) and biogenic OOC, respectively (Huang et al., 2020).~~

415 The particle size dependent variations of HULIS-1 reflected that the contents of the highly oxygenated species in WSOC increased first ~~and decreased afterwards~~ (peaked between 0.26 to 0.44 μm), ~~and then decreased with particle size~~, which cogently confirmed the size-dependent chemical variations composition of WSOC ~~happened with particle size increasing~~. Huang et al., (2020) observed the increase and decrease. Such a finding is consistent with the trend of O/C ratio in size-resolved samples in Shenzhen in a winter, ~~suggesting that these variations did not rely on geographical location~~. (Huang et al., 2020). The variations of HULIS-1 ~~could also verify further suggested~~ that secondary processes were active during the particle formation process, which confirmed ~~the application of that~~ GRD value can be applied as an indicator of the aging state of WSOC.

5 Conclusions and Implications

425 ~~The SFI spectra of coarse mode WSOC were relatively stable and could serve as a referential spectrum of environmental natural sources for other research. The AFI/WSOC ratio in ambient WSOC showed vast distinction with source samples and AFI/WSOC value could be used as a potential indicator of the oxidation degree of secondary WSOC. But considering the representativeness of this ratio, more research on AFI/WSOC ratio from different sources and transformation processes could be implemented in the future.~~

430 ~~The variations of fluorescent characteristics in different particle sizes suggested that the fluorescence method is applicable to the research of the aging process of WSOC. Along with fluorescence indices, extensive information could be addressed in an EEM spectrum. Better understanding the connections between fluorescence property and chemical structure of organic matter, it might be possible to only use EEM data to understand the oxidation state of organics.~~

435 ~~However, the application of EEM method still faces many uncertainties. The seasonal and particle size dependant distinctions of fluorescent WSOC suggested that the sources and transformations of anthropogenic sources were quite different~~

~~in winter and summer, secondary processes could induce fluorescence variations of WSOC. Therefore, future research could take effort to research the fluorescence characteristic of secondary WSOC.~~

6 Conclusion

In this study, a 6 stage MOUDI sampler was adopted to collected size-segregated samples of aerosol particles in a rural site of Beijing. The WSOC concentrations, UV absorption, fluorescence properties, and the energy information of fluorophores of different particle sizes were analyzed. PARAFAC method was used to decompose the mixture of fluorophores. The connections between WSOC and AFI of different particles were analyzed by grey relational degree (GRD). ~~To sum up, the~~ WSOC and AFI showed monomodal distributions in winter and bimodal distributions in summer. The fluorescence efficiency (AFI/WSOC) was higher in winter ~~comparing to than~~ summer and higher in particle sizes $<1.4\ \mu\text{m}$ - ~~than in larger particles~~. The variations of Fluorescence indices HIX and Peak T/Peak C ratio, and the ~~indices reflecting energy states of fluorophores~~ $\eta_{\text{WH}>320}$ indicated that the aromaticity or π -conjugated systems of WSOC increased in ultrafine particles ($<0.44\ \mu\text{m}$) and decreased in the afterwards particle sizes. PARAFAC results showed that HULIS was rich in fine mode and protein-like sources were rich in large particles. The GRD results suggested that fluorescent WSOC in particle sizes between 0.26 to 0.44 μm were highly affected by secondary sources.

The SFI spectra of coarse mode WSOC were relatively stable and could serve as a reference for identifying natural sources of WSOC. The AFI/WSOC ratio in ambient WSOC showed vast distinction from that of source samples, and it could be used as a potential indicator of the oxidation degree of secondary WSOC. More research on AFI/WSOC ratio is recommended for generating representative values for different sources and transformation processes.

The particle size dependent variations of fluorescent characteristics suggested the potential applications of the fluorescence method in investigating the aging processes of WSOC. Along with fluorescence indices, extensive information could be addressed in an EEM spectrum including the fluorescence intensities, the humification degree, the energy state and the sources of WSOC. If the connections between fluorescence property and chemical structure of organic matter are well understood, it might be possible to only use EEM data to understand the oxidation states of organics. The seasonal and particle size dependant variations of fluorescent of WSOC suggested that the sources and transformations of anthropogenic sources were quite different in winter and summer, secondary processes could induce fluorescence variations of WSOC. Therefore, future research could take effort to research the fluorescence characteristic of secondary WSOC.

Author contribution: JT and KX designed the experiments, JQ collected all samples, JQ and YY carried out the experiments. JQ performed data analysis and indices calculation and KX supervised. YQ, XW₂ and SS provided ~~advices~~advice on data analysis and literal problems. XZ, XM, KX₂ and JT provided technical consultations about article writing. JQ prepared the manuscript with contributions from all co-authors.

Acknowledge: This work was supported by the National Natural Science Foundation of China (Grant Nos. 41675127, 41475116). We also appreciate the valuable advice from the editor who greatly improved the manuscript.

470

Disclaimer Competing interests: The authors declare that they have no conflict of interest.

References

- Almeida, A. S., Ferreira, R. M. P., Silva, A. M. S., Duarte, A. C., Neves, B. M. and Duarte, R.: Structural features and pro-
475 inflammatory effects of water-soluble organic matter in inhalable fine urban air particles, *Environ Sci Technol*, 54, 1082–1091,
<https://doi.org/10.1021/acs.est.9b04596>, ~~2019~~2020.
- Andrade-Eiroa, Á., Canle, M. and Cerdá, V.: Environmental applications of excitation-emission spectrofluorimetry: An in-
depth review I, *Applied Spectroscopy Reviews*, 48, 1–49, <https://doi.org/10.1080/05704928.2012.692104>, 2013.
- Asa-Awuku, A., Engelhart, G. J., Lee, B. H., Pandis, S. N. and Nenes, A.: Relating CCN activity, volatility, and droplet growth
480 kinetics of β -caryophyllene secondary organic aerosol, *Atmos. Chem. Phys.*, 9, 795–812, [https://doi.org/10.5194/acp-9-795-](https://doi.org/10.5194/acp-9-795-2009)
[2009](https://doi.org/10.5194/acp-9-795-2009), 2009.
- Bahram, M., Bro, R., Stedmon, C. and Afkhami, A.: Handling of Rayleigh and Raman scatter for PARAFAC modeling of
fluorescence data using interpolation, *J. Chemometr.*, 20, 99–105, <https://doi.org/10.1002/cem.978>, 2006.
- Berberan-Santos, M. N. and Valeur, B.: *Molecular fluorescence: Principles and Applications*, Second Edition, Wiley-VCH,
485 Germany, <https://doi.org/10.1002/9783527650002.index>, 2012.
- Birdwell, J. E. and Engel, A. S.: Characterization of dissolved organic matter in cave and spring waters using UV-Vis
absorbance and fluorescence spectroscopy, *Org. Geochem.*, 41, 270–280, <https://doi.org/10.1016/j.orggeochem.2009.11.002>,
2010.
- Burnett, R., Chen, H., Szyszkowicz, M., Fann, N., Hubbell, B., Pope, C. A., Apte, J. S., Brauer, M., Cohen, A., Weichenthal,
490 S., Coggins, J., Di, Q., Brunekreef, B., Frostad, J., Lim, S. S., Kan, H., Walker, K. D., Thurston, G. D., Hayes, R. B., Lim, C.
C., Turner, M. C., Jerrett, M., Krewski, D., Gapstur, S. M., Diver, W. R., Ostro, B., Goldberg, D., Crouse, D. L., Martin, R.
V., Peters, P., Pinault, L., Tjepkema, M., van Donkelaar, A., Villeneuve, P. J., Miller, A. B., Yin, P., Zhou, M., Wang, L.,
Janssen, N. A. H., Marra, M., Atkinson, R. W., Tsang, H., Quoc Thach, T., Cannon, J. B., Allen, R. T., Hart, J. E., Laden, F.,
Cesaroni, G., Forastiere, F., Weinmayr, G., Jaensch, A., Nagel, G., Concin, H. and Spadaro, J. V.: Global estimates of mortality
495 associated with long-term exposure to outdoor fine particulate matter, *Proc. Natl. Acad. Sci. USA*, 115, 9592,
<https://doi.org/10.1073/pnas.1803222115>, 2018.
- Cai, J., Zeng, X., Zhi, G., Gligorovski, S., Sheng, G., Yu, Z., Wang, X. and Peng, P. a.: Molecular composition and
photochemical evolution of water-soluble organic carbon (WSOC) extracted from field biomass burning aerosols using high-
resolution mass spectrometry, *Atmos. Chem. Phys.*, 20, 6115–6128, <https://doi.org/10.5194/acp-20-6115-2020>, 2020.

- 500 Chalbot, M. G., Chitranshi, P., da Costa, G. G., Pollock, E. and Kavouras, I. G.: Characterization of water-soluble organic matter in urban aerosol by ^1H -NMR spectroscopy, *Atmos. Environ.*, 128, 235-245, <https://doi.org/10.1016/j.atmosenv.2015.12.067>, 2016.
- Chen, Q., Mu, Z., Song, W., Wang, Y., Yang, Z., Zhang, L. and Zhang, Y. L.: Size-resolved characterization of the chromophores in atmospheric particulate matter from a typical coal-burning city in China, *J. of Geophys. Res.: Atmos.*, 124, 10546-10563, <https://doi.org/10.1029/2019jd031149>, 2019.
- 505 Chen, Q. C., Ikemori, F. and Mochida, M.: Light absorption and excitation-emission fluorescence of urban organic aerosol components and their relationship to chemical structure, *Environ. Sci. Technol.*, 50, 10859-10868, <https://doi.org/10.1021/acs.est.6b02541>, 2016a.
- Chen, Q. C., Miyazaki, Y., Kawamura, K., Matsumoto, K., Coburn, S., Volkamer, R., Iwamoto, Y., Kagami, S., Deng, Y. G., Ogawa, S., Ramasamy, S., Kato, S., Ida, A., Kajii, Y. and Mochida, M.: Characterization of chromophoric water-soluble organic matter in urban, forest, and marine aerosols by HR-ToF-MS analysis and excitation emission matrix spectroscopy, *Environ. Sci. Technol.*, 50, 10351-10360, <https://doi.org/10.1021/acs.est.6b01643>, 2016b.
- 510 Cheng, Y., He, K. B., Duan, F. K., Zheng, M., Ma, Y. L. and Tan, J. H.: Measurement of semivolatile carbonaceous aerosols and its implications: A review, *Environ. Int.*, 35, 674-681, <https://doi.org/10.1016/j.envint.2008.11.007>, 2009.
- 515 Coble, P.: Aquatic organic matter fluorescence, New York, US, Cambridge University Press, <https://doi.org/10.1017/CBO9781139045452>, 2014.
- Coble, P. G.: Characterization of marine and terrestrial DOM in seawater using excitation emission matrix spectroscopy, *Mar. Chem.*, 51, 325-346, [https://doi.org/10.1016/0304-4203\(95\)00062-3](https://doi.org/10.1016/0304-4203(95)00062-3), 1996.
- Dasari, S., Andersson, A., Bikkina, S., Holmstrand, H., Budhavant, K., Satheesh, S., Asmi, E., Kesti, J., Backman, J., Salam, A., Bisht, D. S., Tiwari, S., Hameed, Z. and Gustafsson, Ö.: Photochemical degradation affects the light absorption of water-soluble brown carbon in the South Asian outflow, *Sci. Adv.*, 10, <https://doi.org/10.1126/sciadv.aau8066>, 2019.
- 520 De Laurentiis, E., Sur, B., Pazzi, M., Maurino, V., Minero, C., Mailhot, G., Brigante, M. and Vione, D.: Phenol transformation and dimerisation, photosensitised by the triplet state of 1-nitronaphthalene: A possible pathway to humic-like substances (HULIS) in atmospheric waters, *Atmos. Environ.*, 70, 318-327, <https://doi.org/10.1016/j.atmosenv.2013.01.014>, 2013.
- 525 Decesari, S., Facchini, M. C., Matta, E., Lettini, F., Mircea, M., Fuzzi, S., Tagliavini, E. and Putaud, J. P.: Chemical features and seasonal variation of fine aerosol water-soluble organic compounds in the Po Valley, Italy, *Atmos. Environ.*, 35, 3691-3699, [https://doi.org/10.1016/s1352-2310\(00\)00509-4](https://doi.org/10.1016/s1352-2310(00)00509-4), 2001.
- Deng, J.-L.: Control problems of grey systems, *Syst. Control Lett.*, 1, 288-294, [https://doi.org/10.1016/S0167-6911\(82\)80025-X](https://doi.org/10.1016/S0167-6911(82)80025-X), 1982.
- 530 Deshmukh, D. K., Kawamura, K. and Deb, M. K.: Dicarboxylic acids, omega-oxocarboxylic acids, alpha-dicarbonyls, WSOC, OC, EC, and inorganic ions in wintertime size-segregated aerosols from central India: Sources and formation processes, *Chemosphere*, 161, 27-42, <https://doi.org/10.1016/j.chemosphere.2016.06.107>, 2016.

Duarte, R., Pineiro-Iglesias, M., Lopez-Mahia, P., Muniategui-Lorenzo, S., Moreda-Pineiro, J., Silva, A. M. S. and Duarte, A. C.: Comparative study of atmospheric water-soluble organic aerosols composition in contrasting suburban environments in the Iberian Peninsula Coast, *Sci. Total. Environ.*, 648, 430-441, <https://doi.org/10.1016/j.scitotenv.2018.08.171>, 2019.

Duarte, R., Pio, C. A. and Duarte, A. C.: Synchronous scan and excitation-emission matrix fluorescence spectroscopy of water-soluble organic compounds in atmospheric aerosols, *J. Atmos. Chem.*, 48, 157-171, <https://doi.org/10.1023/B:JOCH.0000036845.82039.8c>, 2004.

Duarte, R., Santos, E. B. H., Pio, C. A. and Duarte, A. C.: Comparison of structural features of water-soluble organic matter from atmospheric aerosols with those of aquatic humic substances, *Atmos. Environ.*, 41, 8100-8113, <https://doi.org/10.1016/j.atmosenv.2007.06.034>, 2007.

Duarte, R. M. B. O., Duan, P., Mao, J., Chu, W., Duarte, A. C. and Schmidt-Rohr, K.: Exploring water-soluble organic aerosols structures in urban atmosphere using advanced solid-state ^{13}C -NMR spectroscopy, *Atmos. Environ.*, 230, 117503, <https://doi.org/10.1016/j.atmosenv.2020.117503>, 2020.

Duarte, R. M. B. O., Freire, S. M. S. C. and Duarte, A. C.: Investigating the water-soluble organic functionality of urban aerosols using two-dimensional correlation of solid-state ^{13}C -NMR and FTIR spectral data, *Atmos. Environ.*, 116, 245-252, <https://doi.org/10.1016/j.atmosenv.2015.06.043>, 2015.

Fan, J., Rosenfeld, D., Zhang, Y., Giangrande, S. E., Li, Z., Machado, L. A. T., Martin, S. T., Yang, Y., Wang, J., Artaxo, P., Barbosa, H. M. J., Braga, R. C., Comstock, J. M., Feng, Z., Gao, W., Gomes, H. B., Mei, F., Pöhlker, C., Pöhlker, M. L., Pöschl, U. and Souza, R. A. F. d.: Substantial convection and precipitation enhancements by ultrafine aerosol particles, *Science*, 359, 8, <https://doi.org/10.1126/science.aan8461>, 2020.

Frka, S., Grgić, I., Turšič, J., Gini, M. I. and Eleftheriadis, K.: Seasonal variability of carbon in humic-like matter of ambient size-segregated water-soluble organic aerosols from urban background environment, *Atmos. Environ.*, 173, 239-247, <https://doi.org/10.1016/j.atmosenv.2017.11.013>, 2018.

Fu, P., Kawamura, K., Chen, J. and Miyazaki, Y.: Secondary production of organic aerosols from biogenic VOCs over Mt. Fuji, Japan, *Environ Sci Technol*, 48, 8491-8497, <https://doi.org/10.1021/es500794d>, 2014.

Fu, P., Kawamura, K., Chen, J., Qin, M., Ren, L., Sun, Y., Wang, Z., Barrie, L. A., Tachibana, E., Ding, A. and Yamashita, Y.: Fluorescent water-soluble organic aerosols in the High Arctic atmosphere, *Sci Rep*, 5, <https://doi.org/10.1038/srep09845>, 2015.

Hecobian, A., Zhang, X., Zheng, M., Frank, N., Edgerton, E. S. and Weber, R. J.: Water-Soluble Organic Aerosol material and the light-absorption characteristics of aqueous extracts measured over the Southeastern United States, *Atmos. Chem. Phys.*, 10, 5965-5977, <https://doi.org/10.5194/acp-10-5965-2010>, 2010.

Huang, X. F., Dai, J., Zhu, Q., Yu, K. and Du, K.: Abundant biogenic oxygenated organic aerosol in atmospheric coarse particles: plausible sources and atmospheric implications, *Environ Sci Technol*, 54, 1425-1430, <https://doi.org/10.1021/acs.est.9b06311>, 2020.

- Jang, K.-S., Choi, A. Y., Choi, M., Kang, H., Kim, T.-W. and Park, K.-T.: Size-segregated chemical compositions of HULIS in ambient aerosols collected during the winter season in Songdo, South Korea, *Atmosphere*, 10, 226, <https://doi.org/10.3390/atmos10040226>, 2019.
- Johnston, M. V. and Kerecman, D. E.: Molecular Characterization of Atmospheric Organic Aerosol by Mass Spectrometry, *Annu. Rev. Anal. Chem.*, 12, 247-274, <https://doi.org/10.1146/annurev-anchem-061516-045135>, 2019.
- Kalberer, M., Paulsen, D., Sax, M., Steinbacher, M., Dommen, J., Prevot, A. S. H., Fisseha, R., Weingartner, E., Frankevich, V., and Zenobi, R.: Identification of polymers as major components of atmospheric organic aerosols, *Science*, 303, 1659-1662, <https://doi.org/10.1126/science.1092185>, 2004.
- Kuo, Y., Yang, T. and Huang, G.W.: The use of grey relational analysis in solving multiple attribute decision-making problems, *Comput. Ind. Eng.*, <https://doi.org/10.1016/j.cie.2007.12.002>, 2008.
- Lakowicz, J. R.: Principles of Fluorescence Spectroscopy, Springer US. <https://doi.org/10.1007/978-0-387-46312-4>, 2006.
- Lee, H. J., Aiona, P. K., Laskin, A., Laskin, J. and Nizkorodov, S. A.: Effect of solar radiation on the optical properties and molecular composition of laboratory proxies of atmospheric brown carbon, *Environ. Sci. Technol.*, 48, 10217-10226, <https://doi.org/10.1021/es502515r>, 2014.
- Lee, H. J., Laskin, A., Laskin, J. and Nizkorodov, S. A.: Excitation-emission spectra and fluorescence quantum yields for fresh and aged biogenic secondary organic aerosols, *Environ. Sci. Technol.*, 47, 5763-5770, <https://doi.org/10.1021/es400644c>, 2013.
- Liu, J., Bergin, M., Guo, H., King, L., Kotra, N., Edgerton, E. and Weber, R. J.: Size-resolved measurements of brown carbon in water and methanol extracts and estimates of their contribution to ambient fine-particle light absorption, *Atmos. Chem. Phys.*, 13, 12389-12404, <https://doi.org/10.5194/acp-13-12389-2013>, 2013.
- Masalaite, A., Holzinger, R., Ceburnis, D., Remeikis, V., Ulevicius, V., Rockmann, T. and Dusek, U.: Sources and atmospheric processing of size segregated aerosol particles revealed by stable carbon isotope ratios and chemical speciation, *Environ. Pollut.*, 240, 286-296, <https://doi.org/10.1016/j.envpol.2018.04.073>, 2018.
- Mayorga, R. J., Zhao, Z. and Zhang, H.: Formation of secondary organic aerosol from nitrate radical oxidation of phenolic VOCs: Implications for nitration mechanisms and brown carbon formation, *Atmos. Environ.*, 244, 117910, <https://doi.org/10.1016/j.atmosenv.2020.117910>, 2021.
- Morán, J., Granada, E., Míguez, J. L. and Porteiro, J.: Use of grey relational analysis to assess and optimize small biomass boilers, *Fuel. Process. Technol.*, 87, 123-127, <https://doi.org/10.1016/j.fuproc.2005.08.008>, 2006.
- Murphy, K. R., Hambly, A., Singh, S., Henderson, R. K., Baker, A., Stuetz, R. and Khan, S. J.: Organic matter fluorescence in municipal water recycling schemes: toward a unified PARAFAC model, *Environ. Sci. Technol.*, 45, 2909-2916, <https://doi.org/10.1021/es103015e>, 2011.
- ParkSeungShik, Park S., Yu, J., Yu, G.-H. and 배민석: Chemical and absorption characteristics of water-soluble organic carbon and humic-like substances in size-segregated particles from biomass burning emissions, *Asian J. Atmos. Environ.*, 11, 96-106, <https://doi.org/10.5572/ajae.2017.11.2.096>, 2017.

- 600 Pohlker, C., Huffman, J. A. and Poschl, U.: Autofluorescence of atmospheric bioaerosols-fluorescent biomolecules and potential interferences, *Atmos. Meas. Tech.*, 5, 37-71, <https://doi.org/10.5194/amt-5-37-2012>, 2012.
- Pósfai, M. and Buseck, P. R.: Nature and climate effects of individual tropospheric aerosol particles, *Annu. Rev. Earth. Pl. Sc.*, 38, 17-43, <https://doi.org/10.1146/annurev.earth.031208.100032>, 2010.
- Qin, J., Zhang, L., Zhou, X., Duan, J., Mu, S., Xiao, K., Hu, J. and Tan, J.: Fluorescence fingerprinting properties for exploring
605 water-soluble organic compounds in PM_{2.5} in an industrial city of northwest China, *Atmos. Environ.*, 184, 203-211, <https://doi.org/10.1016/j.atmosenv.2018.04.049>, 2018.
- Qiu, B., Wang, F., Li, Y. and Zuo, W.: Research on method of simulation model validation based on improved grey relational analysis, *Phys. Pro.*, 25, 1118-1125, <https://doi.org/10.1016/j.phpro.2012.03.208>, 2012.
- Santos, P. S. M., Duarte, R. and Duarte, A. C.: Absorption and fluorescence properties of rainwater during the cold season at
610 a town in Western Portugal, *J. Atmos. Chem.*, 62, 45-57, <https://doi.org/10.1007/s10874-009-9138-1>, 2009.
- ~~Soleimanian, E., Mousavi, A., Taghvae, S., Shafer, M. M. and Sioutas, C.: Impact of secondary and primary particulate matter (PM) sources on the enhanced light absorption by brown carbon (BrC) particles in central Los Angeles, *Sci Total Environ*, 705, 135902, <https://doi.org/10.1016/j.scitotenv.2019.135902>, 2020.~~
- Stark, R. E., Yu, B., Zhong, J., Yan, B., Wu, G. and Tian, S.: Environmental NMR: High-resolution Magic-angle Spinning, 2,
615 377-388, <https://doi.org/10.1002/9780470034590.emrstm1340>, 2013.
- Tan, J., Xiang, P., Zhou, X., Duan, J., Ma, Y., He, K., Cheng, Y., Yu, J. and Querol, X.: Chemical characterization of humic-like substances (HULIS) in PM_{2.5} in Lanzhou, China, *Sci Total Environ*, 573, 1481-1490, <https://doi.org/10.1016/j.scitotenv.2016.08.025>, 2016.
- Tian, S., Pan, Y., Liu, Z., Wen, T. and Wang, Y.: Size-resolved aerosol chemical analysis of extreme haze pollution events
620 during early 2013 in urban Beijing, China, *J Hazard Mater*, 279, 452-460, <https://doi.org/10.1016/j.jhazmat.2014.07.023>, 2014.
- Tian, S. L., Pan, Y. P. and Wang, Y. S.: Size-resolved source apportionment of particulate matter in urban Beijing during haze and non-haze episodes, *Atmos. Chem. Phys.*, 16, 1-19, <https://doi.org/10.5194/acp-16-1-2016>, 2016.
- Vione, D., Albinet, A., Barsotti, F., Mekic, M., Jiang, B., Minero, C., Brigante, M. and Gligorovski, S.: Formation of substances with humic-like fluorescence properties, upon photoinduced oligomerization of typical phenolic compounds emitted by
625 biomass burning, *Atmos. Environ.*, 206, 197-207, <https://doi.org/10.1016/j.atmosenv.2019.03.005>, 2019.
- Voliotis, A., Prokeš, R., Lammel, G. and Samara, C.: New insights on humic-like substances associated with wintertime urban aerosols from central and southern Europe: Size-resolved chemical characterization and optical properties, *Atmos. Environ.*, 166, 286-299, <https://doi.org/10.1016/j.atmosenv.2017.07.024>, 2017.
- Wang, H., Zhang, L., Huo, T., Wang, B., Yang, F., Chen, Y., Tian, M., Qiao, B. and Peng, C.: Application of parallel factor
630 analysis model to decompose excitation-emission matrix fluorescence spectra for characterizing sources of water-soluble brown carbon in PM_{2.5}, *Atmos. Environ.*, 223, 117-192, <https://doi.org/10.1016/j.atmosenv.2019.117192>, 2020.

- Wu, C., Wang, G., Li, J., Li, J., Cao, C., Ge, S., Xie, Y., Chen, J., Li, X., Xue, G., Wang, X., Zhao, Z. and Cao, F.: The characteristics of atmospheric brown carbon in Xi'an, inland China: sources, size distributions and optical properties, *Atmos. Chem. Phys.*, 20, 2017-2030, <https://doi.org/10.5194/acp-20-2017-2020>, 2020.
- 635 Xiang, P., Zhou, X. M., Duan, J. C., Tan, J. H., He, K. B., Yuan, C., Ma, Y. L. and Zhang, Y. X.: Chemical characteristics of water-soluble organic compounds (WSOC) in PM_{2.5} in Beijing, China: 2011-2012, *Atmos. Res.*, 183, 104-112, <https://doi.org/10.1016/j.atmosres.2016.08.020>, 2017.
- Xiao, K., Han, B., Sun, J., Tan, J., Yu, J., Liang, S., Shen, Y. and Huang, X.: Stokes shift and specific fluorescence as potential indicators of organic matter hydrophobicity and molecular weight in membrane bioreactors, *Environ Sci Technol*, 53, 8985-8993, <https://doi.org/10.1021/acs.est.9b02114>, 2019.
- 640 ~~Xiao, K., Liang, S., Xiao, A., Lei, T., Tan, J., Wang, X. and Huang, X.: Fluorescence quotient of excitation emission matrices as a potential indicator of organic matter behavior in membrane bioreactors, *Environ. Sci. Wat. Res.*, <https://doi.org/10.1039/C7EW00270J>, 2018.~~
- ~~Xiao, K.,~~ Shen, Y., Liang, S., Tan, J., Wang, X., Liang, P. and Huang, X.: Characteristic regions of the fluorescence excitation-emission matrix (EEM) to identify hydrophobic/hydrophilic contents of organic matter in membrane bioreactors, *Environ Sci Technol*, 52, 11251-11258, <https://doi.org/10.1021/acs.est.8b02684>, ~~2018~~2018b.
- 645 Xiao, K., Sun, J.-Y., Shen, Y.-X., Liang, S., Liang, P., Wang, X.-M. and Huang, X.: Fluorescence properties of dissolved organic matter as a function of hydrophobicity and molecular weight: case studies from two membrane bioreactors and an oxidation ditch, *RSC Advances*, 6, 24050-24059, <https://doi.org/10.1039/C5RA23167A>, 2016.
- 650 Xiao, K., Yu, J., Wang, S., Du, J., Tan, J., Xue, K., Wang, Y. and Huang, X.: Relationship between fluorescence excitation-emission matrix properties and the relative degree of DOM hydrophobicity in wastewater treatment effluents, *Chemosphere*, 254, 126830, <https://doi.org/10.1016/j.chemosphere.2020.126830>, 2020.
- Xie, X., Chen, Y., Nie, D., Liu, Y., Liu, Y., Lei, R., Zhao, X., Li, H. and Ge, X.: Light-absorbing and fluorescent properties of atmospheric brown carbon: A case study in Nanjing, China, *Chemosphere*, 251, 126350, <https://doi.org/10.1016/j.chemosphere.2020.126350>, 2020.
- 655 Xu, J. A., Sheng, G. P., Luo, H. W., Fang, F., Li, W. W., Zeng, R. J., Tong, Z. H. and Yu, H. Q.: Evaluating the influence of process parameters on soluble microbial products formation using response surface methodology coupled with grey relational analysis, *Water Res.*, 45, 674-680, <https://doi.org/10.1016/j.watres.2010.08.032>, 2011.
- Yan, C., Nie, W., Vogel, A. L., Dada, L., Lehtipalo, K., Stolzenburg, D., Wagner, R., Rissanen, M. P., Xiao, M., Ahonen, L., Fischer, L., Rose, C., Bianchi, F., Gordon, H., Simon, M., Heinritzi, M., Garmash, O., Roldin, P., Dias, A., Ye, P., Hofbauer, V., Amorim, A., Bauer, P. S., Bergen, A., Bernhammer, A.-K., Breitenlechner, M., Brilke, S., Buchholz, A., Mazon, S. B., Canagaratna, M. R., Chen, X., Ding, A., Dommen, J., Draper, D. C., Duplissy, J., Frege, C., Heyn, C., Guida, R., Hakala, J., Heikkinen, L., Hoyle, C. R., Jokinen, T., Kangasluoma, J., Kirkby, J., Kontkanen, J., Kürten, A., Lawler, M. J., Mai, H., Mathot, S., Mauldin, R. L., Molteni, U., Nichman, L., Nieminen, T., Nowak, J., Ojdanic, A., Onnela, A., Pajunoja, A., Petäjä, T., Piel, F., Quéléver, L. L. J., Sarnela, N., Schallhart, S., Sengupta, K., Sipilä, M., Tomé, A., Tröstl, J., Väisänen, O., Wagner,
- 665

- A. C., Ylisirniö, A., Zha, Q., Baltensperger, U., Carslaw, K. S., Curtius, J., Flagan, R. C., Hansel, A., Riipinen, I., Smith, J. N., Virtanen, A., Winkler, P. M., Donahue, N. M., Kerminen, V.-M., Kulmala, M., Ehn, M. and Worsnop, D. R.: Size-dependent influence of NO_x on the growth rates of organic aerosol particles, *Sci. Adv.*, 6, eaay4945, <https://doi.org/10.1126/sciadv.aay4945>, 2020.
- 670 You, M. L., Shu, C. M., Chen, W. T. and Shyu, M. L.: Analysis of cardinal grey relational grade and grey entropy on achievement of air pollution reduction by evaluating air quality trend in Japan, *J. Clean Prod.*, 142, 3883-3889, <https://doi.org/10.1016/j.jclepro.2016.10.072>, 2017.
- Yu, G. H., Park, S. and Lee, K. H.: Source contributions and potential source regions of size-resolved water-soluble organic carbon measured at an urban site over one year, *Environ. Sci. Process. Impacts.*, 18, 1343-1358, <https://doi.org/10.1039/c6em00416d>, 2016.
- 675 Yu, J. Z., Yang, H., Zhang, H. Y. and Lau, A. K. H.: Size distributions of water-soluble organic carbon in ambient aerosols and its size-resolved thermal characteristics, *Atmos. Environ.*, 38, 1061-1071, <https://doi.org/10.1016/j.atmosenv.2003.10.049>, 2004.
- Yu, Q., Chen, J., Qin, W., Cheng, S., Zhang, Y., Ahmad, M. and Ouyang, W.: Characteristics and secondary formation of water-soluble organic acids in PM₁, PM_{2.5} and PM₁₀ in Beijing during haze episodes, *Sci. Total. environ.*, 669, 175-184, <https://doi.org/10.1016/j.scitotenv.2019.03.131>, 2019.
- 680 Yue, S., Ren, L., Song, T., Li, L., Xie, Q., Li, W., Kang, M., Zhao, W., Wei, L., Ren, H., Sun, Y., Wang, Z., Ellam, R. M., Liu, C. Q., Kawamura, K. and Fu, P.: Abundance and Diurnal Trends of Fluorescent Bioaerosols in the Troposphere over Mt. Tai, China, in *Spring, J. Geophys. Res.-Atmos.*, 124, 4158-4173, <https://doi.org/10.1029/2018jd029486>, 2019.
- 685 Zanca, N., Lambe, A. T., Massoli, P., Paglione, M., Croasdale, D. R., Parmar, Y., Tagliavini, E., Gilardoni, S. and Decesari, S.: Characterizing source fingerprints and ageing processes in laboratory-generated secondary organic aerosols using proton-nuclear magnetic resonance (¹H-NMR) analysis and HPLC HULIS determination, *Atmos. Chem. Phys.*, 17, 10405-10421, <https://doi.org/10.5194/acp-17-10405-2017>, 2017.
- Zhang, X., Liu, Z., Hecobian, A., Zheng, M., Frank, N. H., Edgerton, E. S., Weber, R. J.: Spatial and seasonal variations of fine particle water-soluble organic carbon (WSOC) over the southeastern United States: implications for secondary organic aerosol formation, *Atmos. Chem. Phys.*, 12, 6593-6607, <https://doi.org/10.5194/acp-12-6593-2012>, 2012.
- 690 Zhang, X., Xu, J., Kang, S., Liu, Y. and Zhang, Q.: Chemical characterization of long-range transport biomass burning emissions to the Himalayas: insights from high-resolution aerosol mass spectrometry, *Atmos. Chem. Phys.*, 18, 4617-4638, <https://doi.org/10.5194/acp-18-4617-2018>, 2018.
- 695 Zhao, W., Fu, P., Yue, S., Li, L., Xie, Q., Zhu, C., Wei, L., Ren, H., Li, P., Li, W., Sun, Y., Wang, Z., Kawamura, K. and Chen, J.: Excitation-emission matrix fluorescence, molecular characterization and compound-specific stable carbon isotopic composition of dissolved organic matter in cloud water over Mt. Tai, *Atmos. Environ.*, 213, 608-619, <https://doi.org/10.1016/j.atmosenv.2019.06.034>, 2019.

Table 1 Size-segregated average WSOC, WSIN concentrations, and their standard ~~divisions~~deviations.

	Species (mg·m ⁻³)	<0.26 <u>μm</u>	0.26-0.44 <u>μm</u>	0.44-0.77 <u>μm</u>	0.77-1.4 <u>μm</u>	1.4-2.5 <u>μm</u>	2.5-10 <u>μm</u>
Winter	Cl ⁻	0.42±0.25	1.36±1.21	0.83±0.72	1.03±0.98	1.19±1.27	0.43±0.45
	NO ₃ ⁻	2.08±1.43	9.42±8.46	5.64±5.61	7.37±8.9	6.72±9.44	1.92±3.28
	SO ₄ ²⁻	1.05±0.6	4.36±3.87	3.21±3.68	5.44±9.43	4.68±7.03	1.18±1.52
	Na ⁺	0.12±0.05	0.21±0.1	0.16±0.08	0.2±0.1	0.52±0.6	0.24±0.25
	NH ₄ ⁺	1.05±0.57	2.9±2.15	2.05±1.82	2.4±2.77	1.67±2.18	0.44±0.67
	Mg ²⁺	0.01	0.01	0.02±0.01	0.05±0.04	0.18±0.21	0.08±0.09
	Ca ²⁺	0.06±0.01	0.11±0.03	0.15±0.08	0.4±0.25	1.67±1.35	0.93±0.9
	K ⁺	0.08±0.04	0.37±0.3	0.24±0.24	0.25±0.25	0.18±0.18	0.05±0.06
	OC	4.49±1.93	11.04±7.2	5.67±4.49	5.45±6.26	5.07±3.88	3.4±5.17
	EC	0.38±0.18	0.93±0.47	0.67±0.43	0.72±0.69	0.62±0.78	1.65±4.37
	WSOC	1.66±0.7	4.73±2.96	2.96±2.41	3.21±4.33	2.31±2.55	0.64±0.5
	WSOC/OC	0.38±0.07	0.43±0.07	0.56±0.27	0.51±0.15	0.37±0.14	0.24±0.25
Summer	Cl ⁻	0.05±0.02	0.1±0.04	0.07±0.03	0.07±0.02	0.16±0.1	0.11±0.06
	NO ₃ ⁻	0.48±0.44	3.5±3.32	1.37±1.35	1.04±0.86	4.76±4.22	1.49±1.37
	SO ₄ ²⁻	1.63±1.18	7.14±6.64	2.59±2.42	1.28±1.13	0.72±0.51	0.2±0.12
	Na ⁺	0.29±0.08	0.37±0.17	0.25±0.06	0.23±0.06	0.27±0.09	0.19±0.03
	NH ₄ ⁺	0.79±0.53	2.56±1.99	1.18±1.02	0.63±0.55	0.5±0.46	0.1±0.08
	Mg ²⁺	0.01	0.01	0.01	0.02±0.01	0.12±0.08	0.05±0.03
	Ca ²⁺	0.05±0.01	0.08±0.02	0.08±0.03	0.16±0.09	1.21±0.87	0.62±0.49
	K ⁺	0.03±0.02	0.14±0.11	0.05±0.04	0.04±0.02	0.06±0.02	0.02±0.01
	OC	2.67±0.98	3.93±2.22	1.39±0.67	1.14±0.41	3.5±1.21	2.22±1.76
	EC	0.38±0.12	0.44±0.16	0.2±0.09	0.22±0.06	0.34±0.22	0.5±0.52
	WSOC	0.67±0.25	1.27±0.86	0.46±0.31	0.33±0.21	0.57±0.18	0.27±0.18
	WSOC/OC	0.26±0.08	0.3±0.07	0.31±0.1	0.27±0.1	0.17±0.04	0.16±0.12

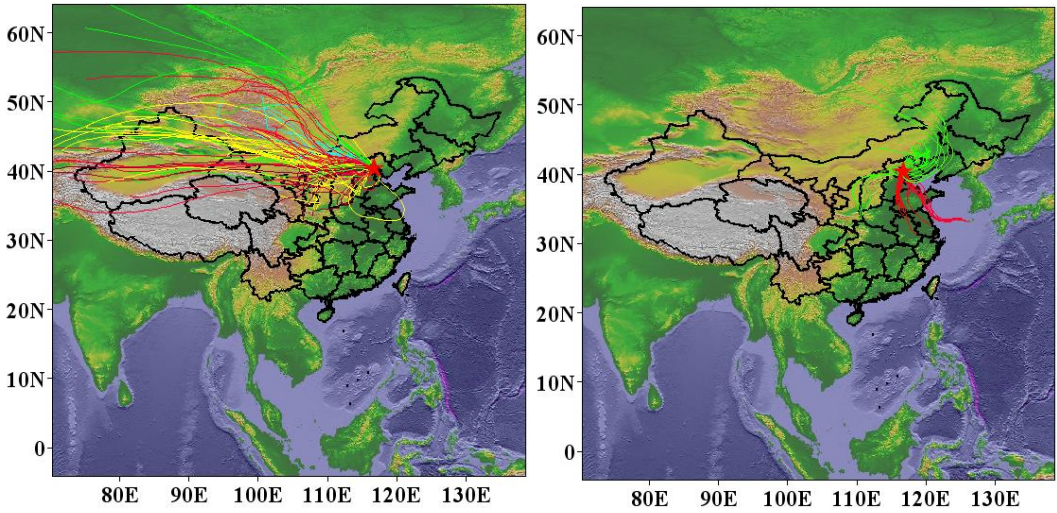
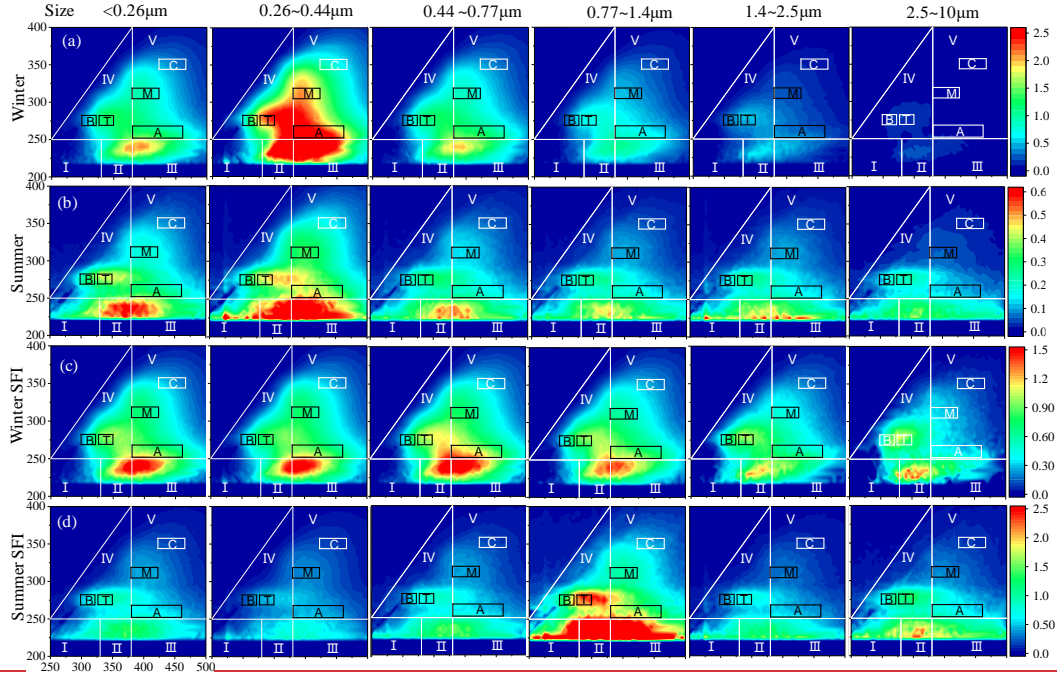


Figure 1 The sampling site and air quality index (AQI) weighted 72 h backward trajectory of winter and summer sampling days, respectively.



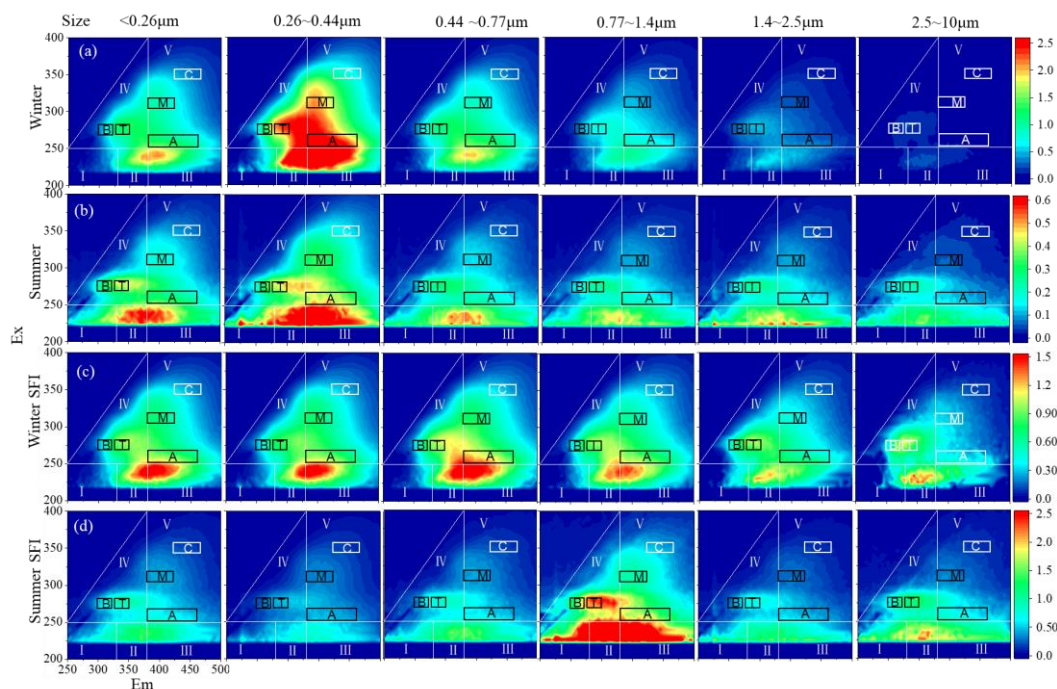


Figure 2 Excitation-emission spectra of size-segregated samples in winter and summer. All spectra were partitioned into five regions and assigned as protein-like pollutants (I and II), fulvic acid (III), soluble microbial byproduct-like substances (IV), and humic-like acid (V), respectively (Birdwell and Engel 2010). Peak A, B, C, M, and T were generally considered as humic-like fluorophores, tyrosine-like ~~fluorophore~~fluorophores, humic-like carbon with larger molecular weight, marine humic-like fluorophore, and tryptophan-like fluorophores (Coble 1996). (a) and (b) were the size-segregated EEM spectra of winter and summer samples, respectively (R.U.), (c), and (d) were the corresponding EEM spectra of fluorescence emitted per unit of WSOC.

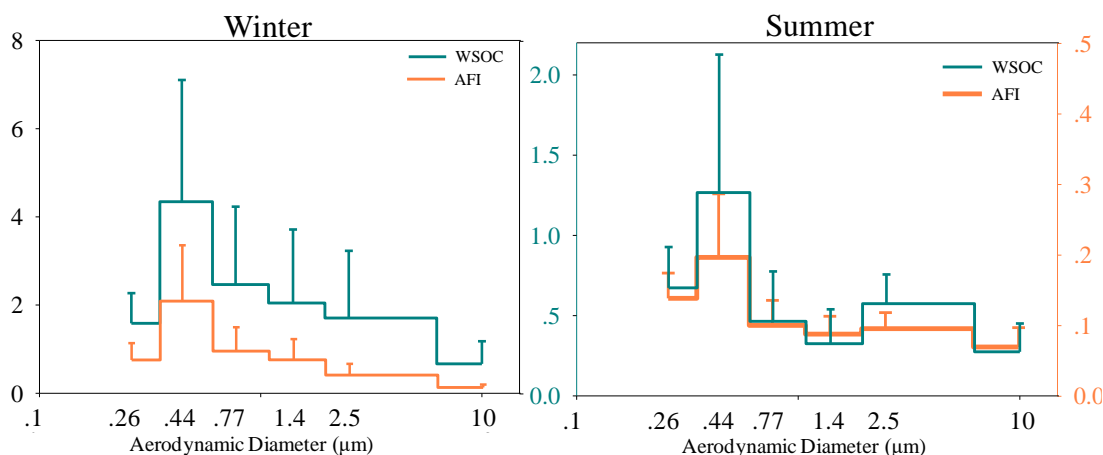
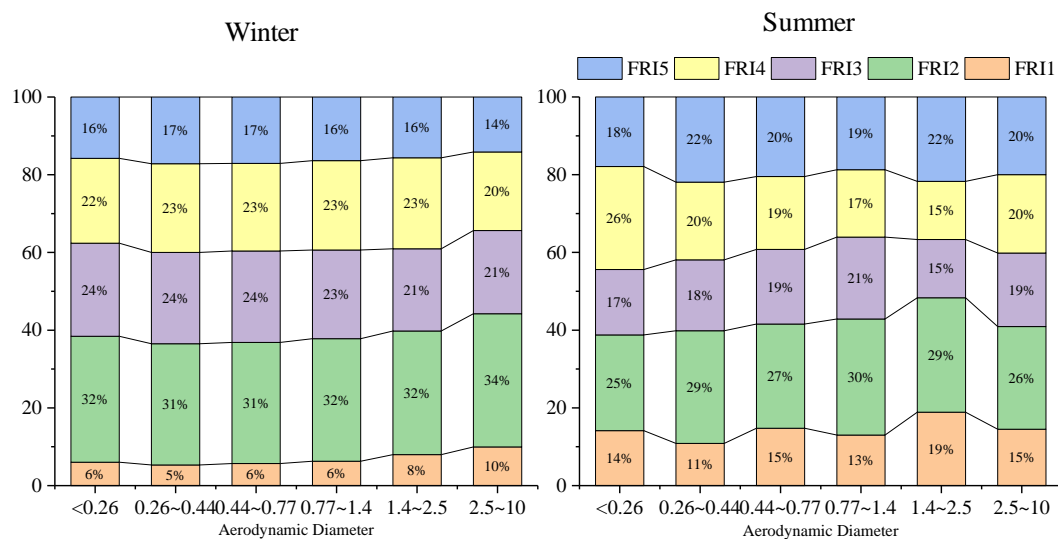
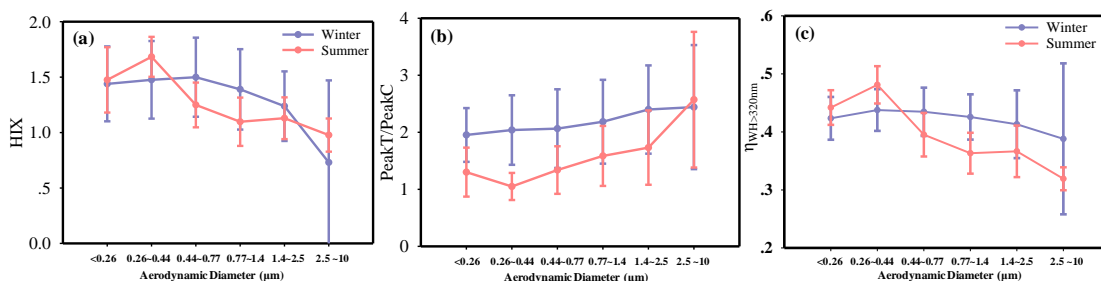


Figure 3 Size distributions of WSOC and AFI in winter and summer. AFI was in ~~Roman~~the Raman unit.



720 **Figure 4** Size distribution of fluorescence regional intensity for winter and summer. FRI1-FRI5 was FRI of fluorescence region I to V.



725 **Figure 5** Humic index and Peak T/Peak C ratio served as indicators of humification degree and the biodegradable possibility of WSOC. (a) HIX in different particle sizes, large HIX value indicated high humification degree or high aromaticity of fluorescent organics. (b) Peak T/Peak C ratios of different particle sizes. The large value indicated more microbial metabolites in the fluorescent organics. (c) showed the size distributions of $\eta_{WH>320nm}$ for winter and summer samples, respectively.

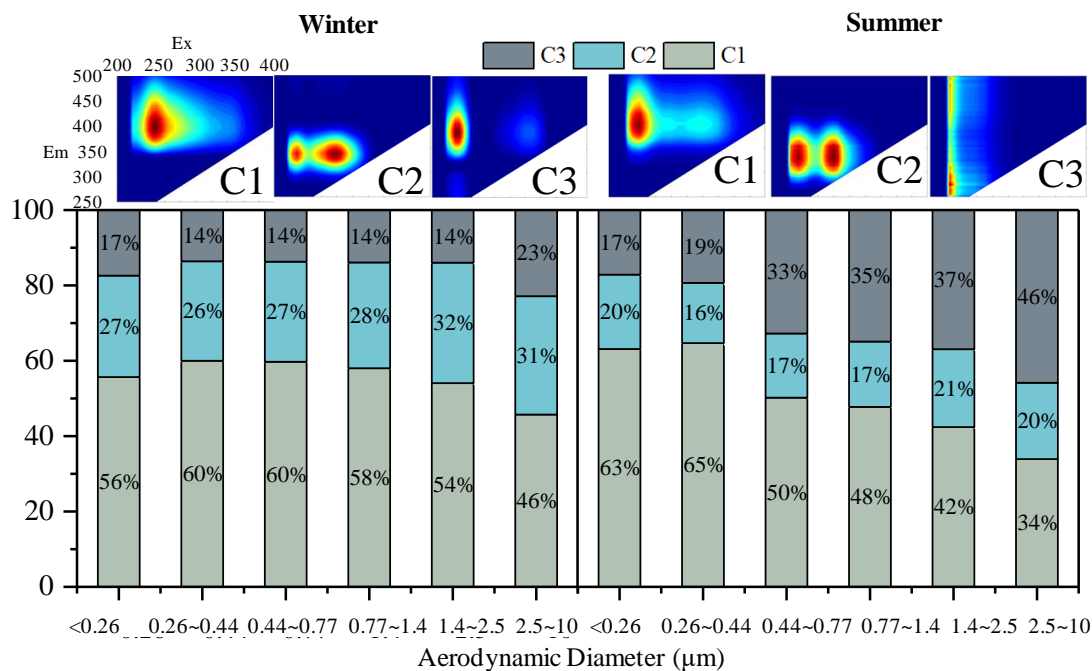


Figure 6 PARAFAC results of EEM in winter and summer respectively. Three components were extracted of both seasons, the portions of each component for different particle sizes were shown as well.

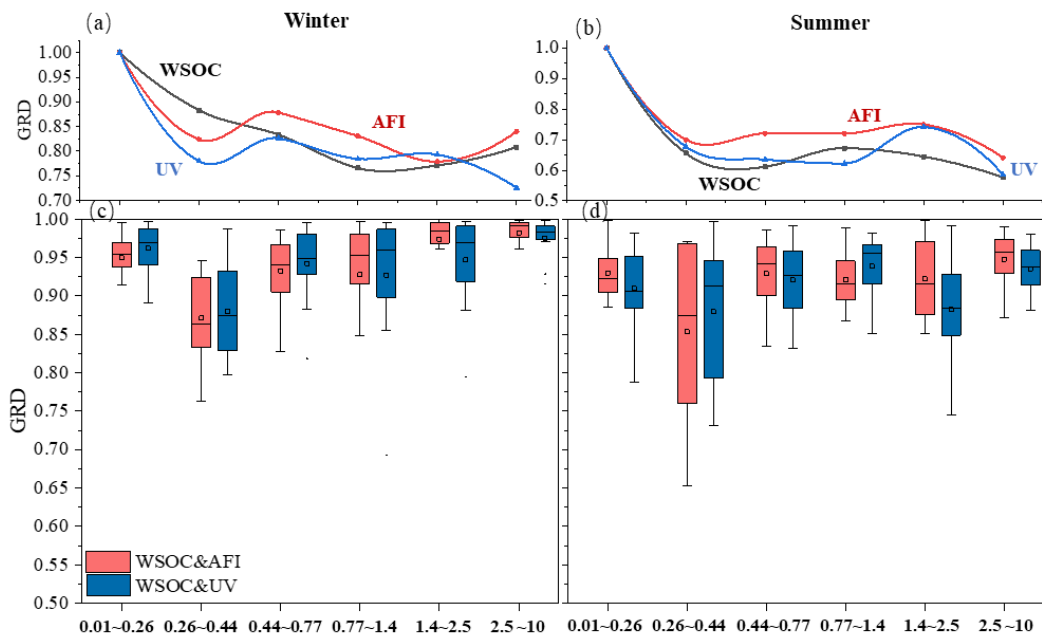


Figure 7 Grey relational degree (GRD) of size-segregated WSOC, AFI, and average UV. (a) and (b) GRD calculated by WSOC, AFI, and average UV of each sample, setting data of 0.01 to 0.26 as references, GRD (0.01-0.26) =1; (c) and (d) GRD between WSOC and light absorption indices, setting WSOC as references.

735